Supplementary Information for

Developing sustainable FeTi alloys for hydrogen storage by recycling

Yuanyuan Shang[1], Shaofei Liu[2], Zhida Liang[3, 4], Florian Pyczak[3], Zhifeng Lei[5], Tim Heidenreich[1], Alexander Schökel[6], Ji-jung Kai[2, 7], Gökhan Gizer[1], Martin Dornheim[1], Thomas Klassen[1, 8], Claudio Pistidda[1]*

[1] Department of Materials Design, Institute of Hydrogen Technology, Helmholtz-Zentrum hereon GmbH, 21502, Geesthacht, Germany

[2] Department of Mechanical Engineering, City University of Hong Kong, 999077, Hong Kong, China

[3] Institute of Materials Research, Helmholtz-Zentrum hereon GmbH, 21502, Geesthacht, Germany

[4] Department of Materials Science and Metallurgy, Cambridge University, Cambridge, CB3 0FS, UK

[5] College of Materials Science and Engineering, Hunan University, 410082, Changsha, China

[6] Deutsches Elektronen-Synchrotron DESY, Notkestr. 85, 22607, Hamburg, Germany

[7] Center for Advanced Nuclear Safety and Sustainable Development, City University of Hong Kong, Hong Kong, China

[8] Helmut Schmidt University, Holstenhofweg 85, 22043, Hamburg, Germany

*Correspondence to: claudio.pistidda@hereon.de, Tel: +49-0-4152-2644

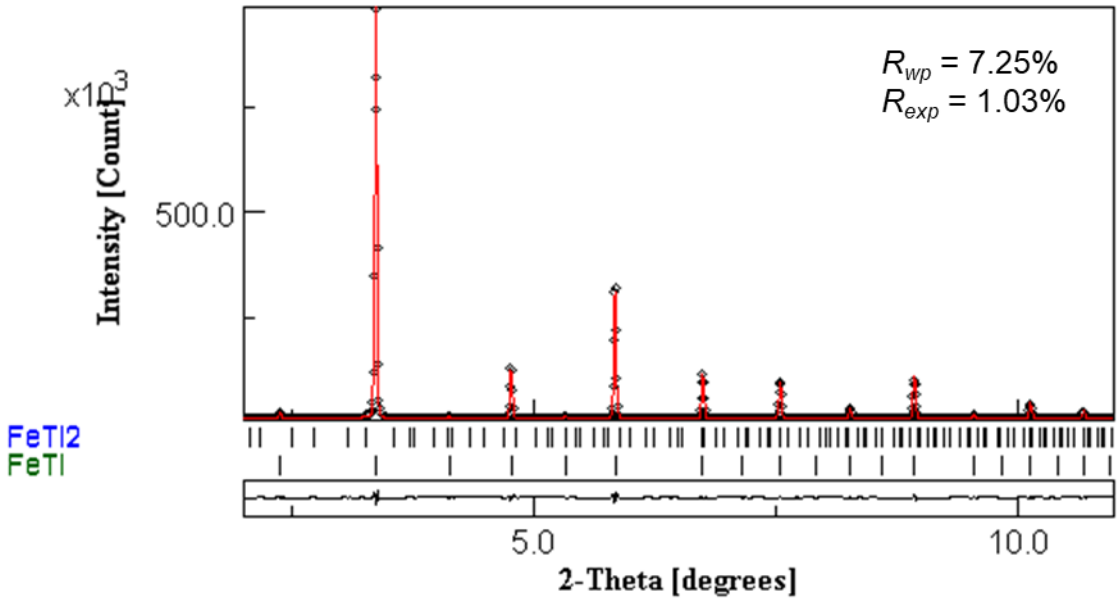

Supplementary Fig. 1 | Rietveld refinement results of as-cast pure FeTi alloy by Maud (λ = 0.124 Å).

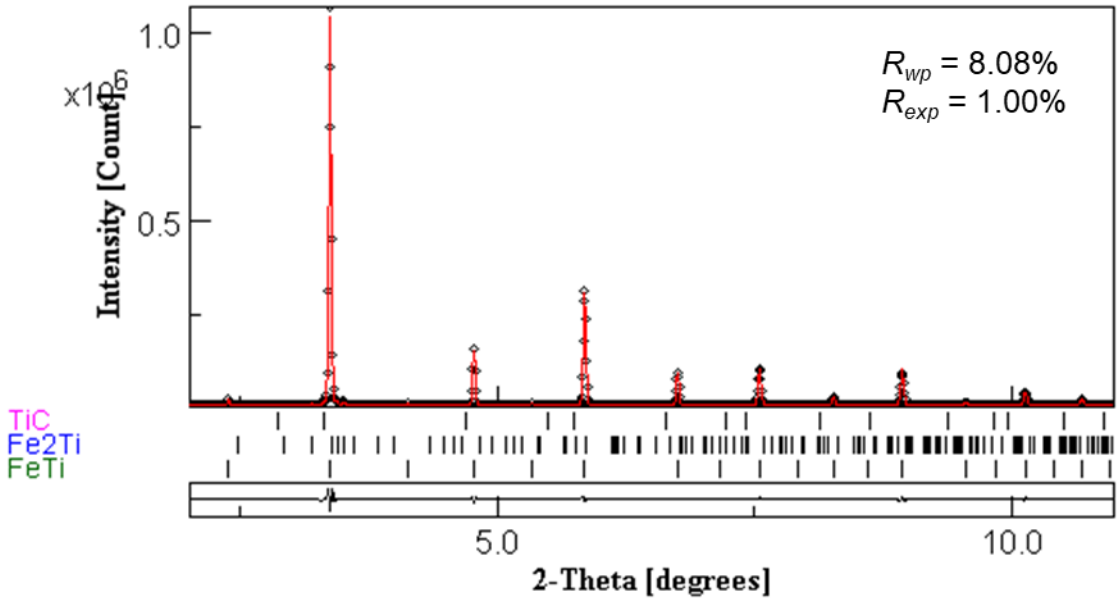

Supplementary Fig. 2 | Rietveld refinement results of as-cast C45-Gr2 FeTi alloy by Maud (λ = 0.124 Å).

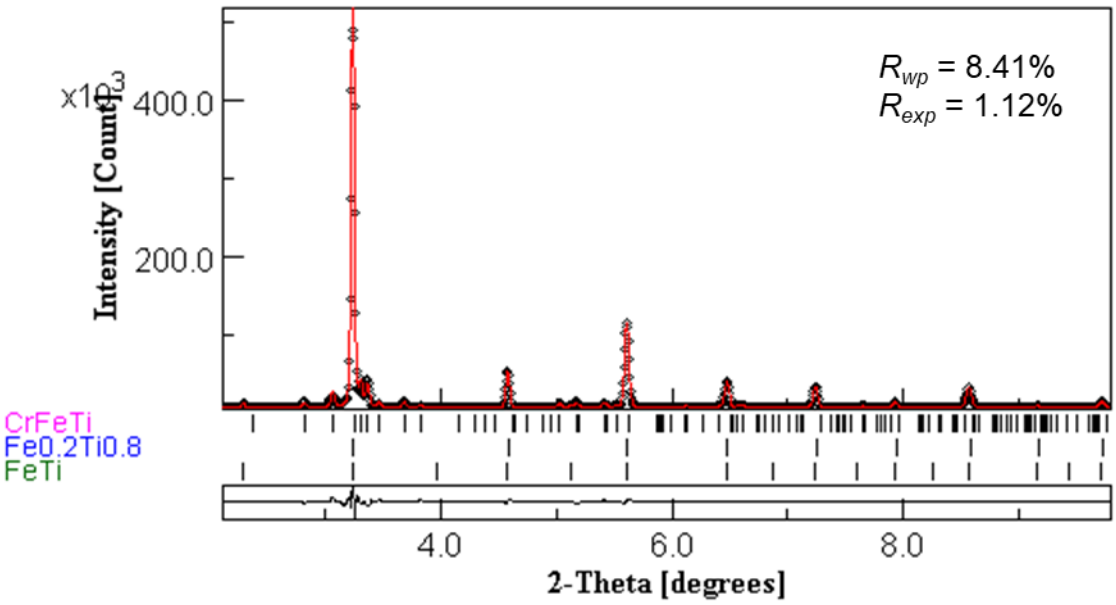

Supplementary Fig. 3 | Rietveld refinement results of as-cast 316L-Gr2 FeTi alloy by Maud (λ = 0.124 Å).

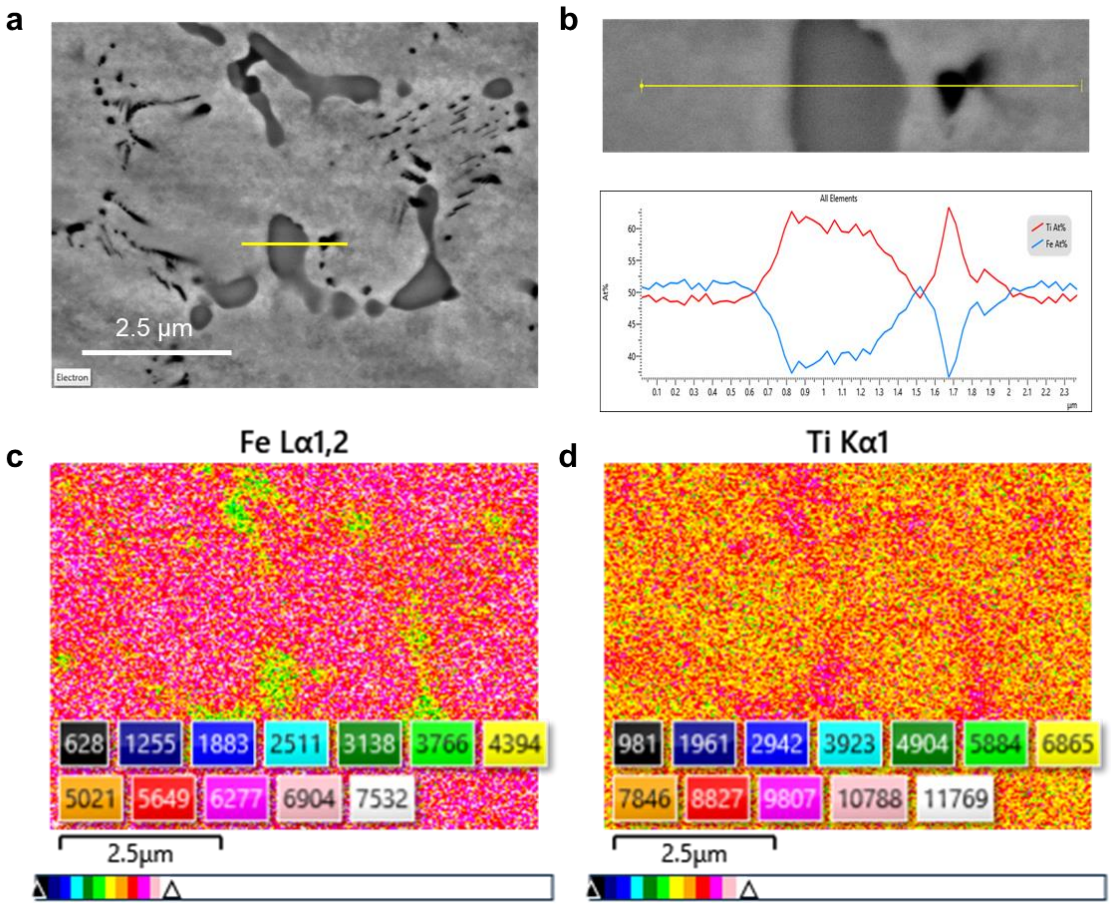

Supplementary Fig. 4 | SEM images of as-cast pure FeTi alloy. a, SEM image. **b**, EDX line profiles of the region selected in **a**. **c**, corresponding EDX mapping of Fe element. **d**, corresponding EDX mapping of Ti element.

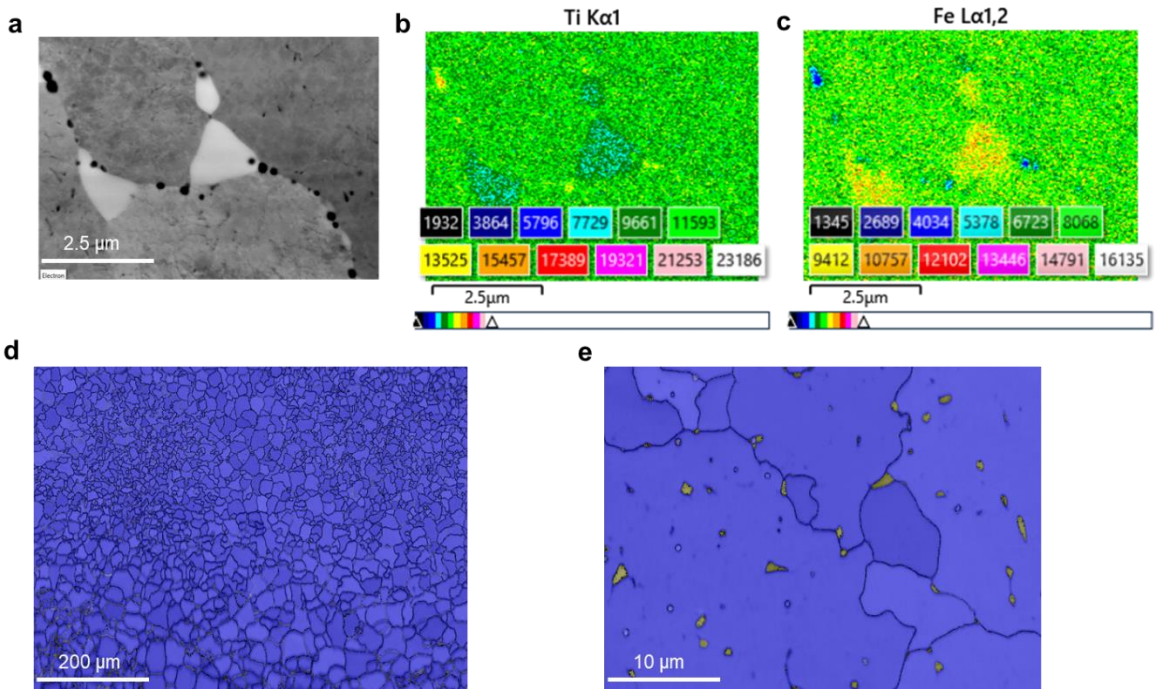

Supplementary Fig. 5 | SEM and EBSD images of as-cast C45-Gr2 FeTi alloy. a, SEM image. **b**, corresponding EDX mapping of Ti element. **c**, corresponding EDX mapping of Fe element. **d** and **e**, EBSD mappings of the alloy.

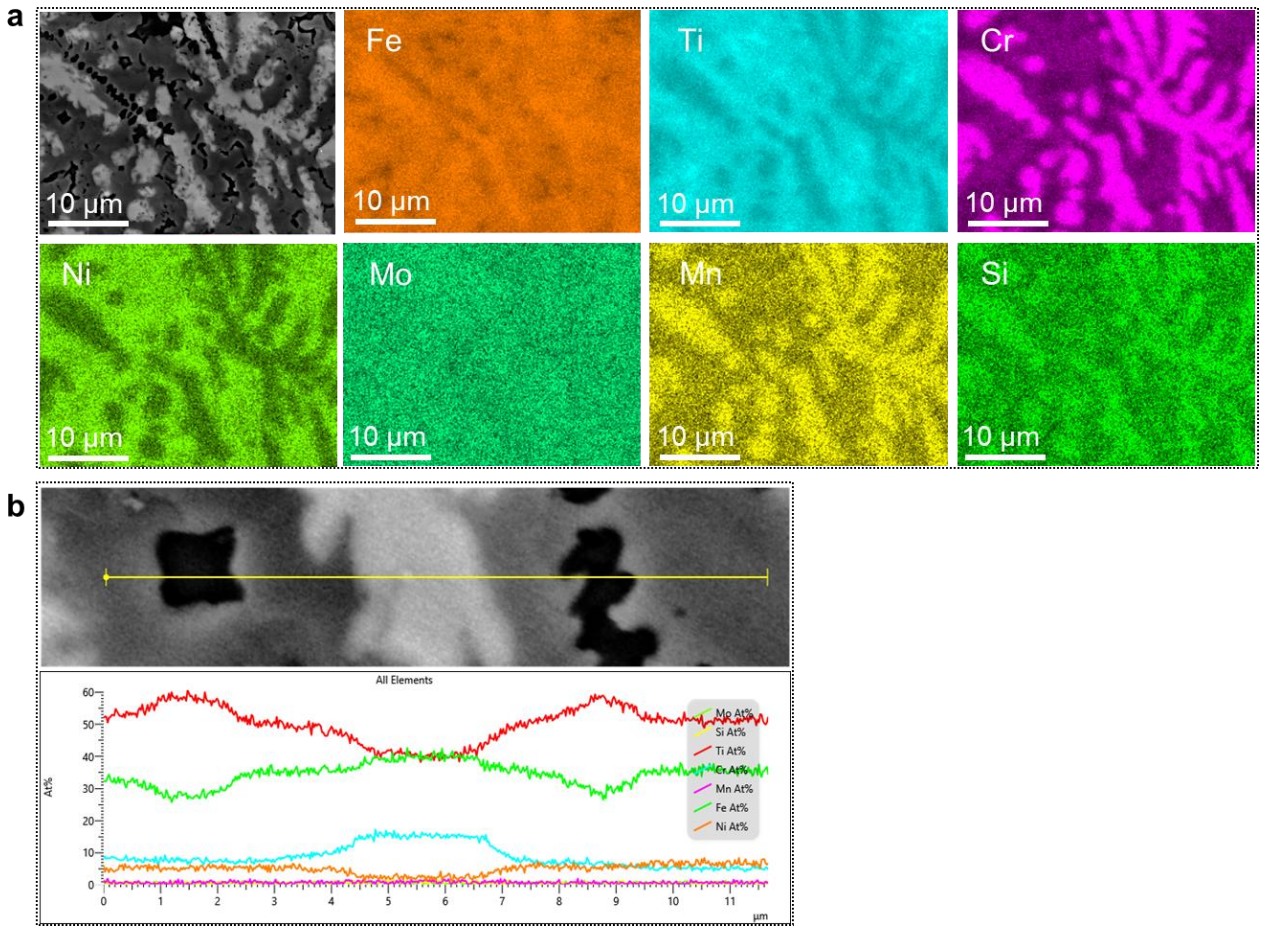

Supplementary Fig. 6 | SEM images of as-cast 316L-Gr2 FeTi alloy. a, SEM image and corresponding EDX mapping of different elements. **b**, EDX line profiles and distribution of different elements.

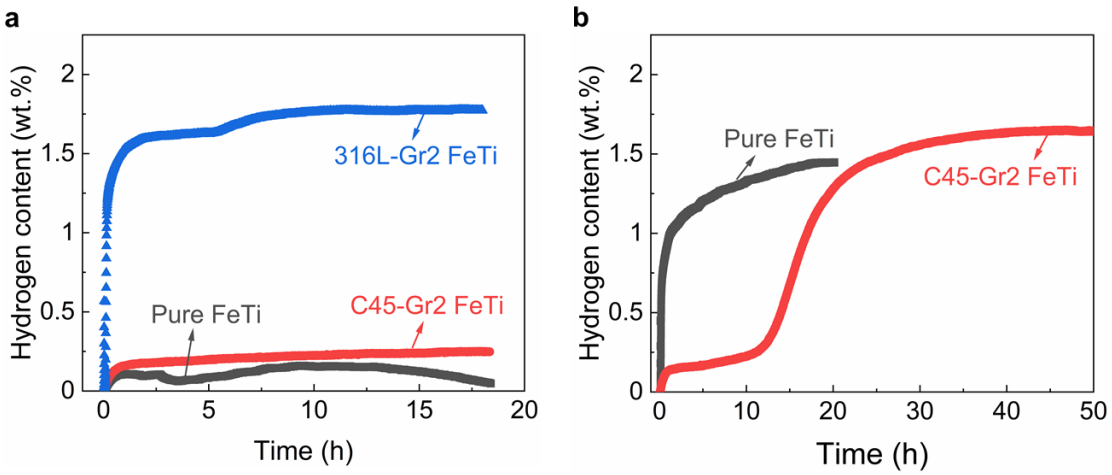

Supplementary Fig. 7 | Activation curves of pure, C45-Gr2 and 316L-Gr2 FeTi alloys at 50 °C and under 65 bar of H_2. a, activation curves of all three samples after being evacuated at 90 °C for 15 h. **b**, activation curves of the pure and C45-Gr2 FeTi alloys after an extra evacuation (3 h) at 90 °C. After the first activation process in **a**, the pure and C45-Gr2 FeTi alloys were not fully activated, so the two samples were evacuated for an extra 3 h.

Supplementary Table 1 | Composition of C45 steel scraps.

Elements	Ni	Cr	Mo	Ni + Cr + Mo	Si	Mn	C	S	P	Fe
Content (wt.%)	≤ 0.40	≤ 0.40	≤ 0.10	≤ 0.63	≤ 0.40	0.50 ~ 0.80	0.42 ~ 0.50	≤ 0.045	≤ 0.045	Rest

Supplementary Table 2 | Composition of 316L steel scraps.

Elements	Ni	Cr	Mo	Si	Mn	C	S	P	N	Fe
Content (wt.%)	10.00 ~ 14.00	16.00 ~ 18.00	2.00 ~ 3.00	≤ 0.75	≤ 2.00	≤ 0.03	≤ 0.03	≤ 0.045	≤ 0.10	Rest

Supplementary Table 3 | Composition of 3.7035 Titanium Grade 2 alloy scraps.

Elements	Fe	C	O	H	N	Ti
Content (wt.%)	≤ 0.30	≤ 0.08	≤ 0.25	≤ 0.015	≤ 0.03	Rest

Supplementary Table 4 | Kinetic fitting results of different models for pure FeTi alloy.

Equation	y = a + b*x										
Plot	D1	D2	D3	D4	**F 1**	R2	R3	F2	F3	F4	F5
Weight	No Weighting										
Intercept	-0.30081 ± 0.03035	-0.44366 ± 0.02316	-0.63023 ± 0.03015	-0.50369 ± 0.02286	**0.00286 ± 0.02258**	0.13867 ± 0.03153	0.09582 ± 0.02891	0.45683 ± 0.02431	0.62444 ± 0.01969	0.71278 ± 0.01617	0.55593 ± 0.0219
Slope	1.26416 ± 0.02972	1.44372 ± 0.02267	1.6857 ± 0.02952	1.52095 ± 0.02238	**0.9666 ± 0.02211**	0.80865 ± 0.03087	0.85784 ± 0.0283	0.50267 ± 0.0238	0.34201 ± 0.01927	0.2596 ± 0.01583	0.40676 ± 0.02144
Residual Sum of Squares	0.0586	0.0341	0.05783	0.03325	**0.03243**	0.06323	0.05316	0.03758	0.02465	0.01662	0.0305
Pearson's r	0.99506	0.99779	0.99725	0.99806	**0.99533**	0.98714	0.99034	0.98042	0.9726	0.96814	0.9759
R-Square (COD)	0.99015	0.99558	0.99451	0.99612	**0.99067**	0.97444	0.98078	0.96122	0.94594	0.93729	0.95238
Adj. R-Square	0.98961	0.99534	0.99421	0.9959	**0.99016**	0.97302	0.97972	0.95907	0.94294	0.93381	0.94974

Supplementary Table 5 | Kinetic fitting results of different models for C45-Gr2 FeTi alloy.

Equation	y = a + b*x										
Plot	D1	D2	D3	D4	F 1	R2	**R3**	F2	F3	F4	F5
Weight	No Weighting										
Intercept	-0.41727 ± 0.01912	-0.5726 ± 0.02198	-0.77523 ± 0.04592	-0.63781 ± 0.02825	-0.08646 ± 0.01203	0.06124 ± 0.02348	**0.01463 ± 0.01999**	0.40781 ± 0.01984	0.59049 ± 0.01697	0.68679 ± 0.01423	0.51583 ± 0.01851
Slope	1.41183 ± 0.0193	1.60791 ± 0.02219	1.87133 ± 0.04636	1.69205 ± 0.02851	1.07981 ± 0.01214	0.90632 ± 0.02371	**0.96042 ± 0.02018**	0.56437 ± 0.02003	0.38464 ± 0.01713	0.2922 ± 0.01436	0.45715 ± 0.01869
Residual Sum of Squares	0.01995	0.02638	0.1151	0.04354	0.0079	0.0301	**0.02181**	0.02148	0.01571	0.01105	0.0187
Pearson's r	0.99832	0.99829	0.99452	0.99745	0.99886	0.9939	**0.99605**	0.98885	0.98262	0.97894	0.98529
R-Square (COD)	0.99665	0.99658	0.98907	0.99491	0.99773	0.98783	**0.99212**	0.97783	0.96553	0.95832	0.9708
Adj. R-Square	0.99646	0.99639	0.98847	0.99463	0.9976	0.98716	**0.99168**	0.9766	0.96362	0.956	0.96918

Supplementary Table 6 | Kinetic fitting results of different models for 316L-Gr2 FeTi alloy.

Equation	y = a + b*x										
Plot	D1	D2	D3	D4	F 1	R2	R3	**F2**	F3	F4	F5
Weight	No Weighting										
Intercept	-1.65867 ± 0.04514	-1.97506 ± 0.08041	-2.39249 ± 0.1398	-2.10902 ± 0.09845	-1.03808 ± 0.02167	-0.74531 ± 0.01976	-0.8373 ± 0.01548	**-0.09753 ± 0.02003**	0.2442 ± 0.01984	0.42299 ± 0.01752	0.10516 ± 0.02058
Slope	2.65207 ± 0.04627	3.00852 ± 0.08242	3.48569 ± 0.1433	3.16107 ± 0.10091	2.03065 ± 0.02221	1.7126 ± 0.02025	1.81192 ± 0.01587	**1.06968 ± 0.02053**	0.73101 ± 0.02033	0.55609 ± 0.01795	0.86787 ± 0.0211
Residual Sum of Squares	0.03243	0.10288	0.31101	0.15425	0.00747	0.00621	0.00381	**0.00638**	0.00626	0.00488	0.00674
Pearson's r	0.99727	0.99331	0.98513	0.99095	0.99892	0.99874	0.99931	**0.9967**	0.99311	0.99075	0.99472
R-Square (COD)	0.99455	0.98667	0.97048	0.98199	0.99785	0.99749	0.99862	**0.99341**	0.98626	0.98158	0.98948
Adj. R-Square	0.99425	0.98593	0.96884	0.98098	0.99773	0.99735	0.99854	**0.99305**	0.9855	0.98056	0.98889

Supplementary Table 7 | Kinetic models used for fitting.

Model types	Kinetic rate models	Equations used for the fitting
Diffusion models	D1 one-dimensional diffusion	$\frac{\alpha^2}{0.25}$
	D2 two-dimensional diffusion	$\frac{\alpha + (1-\alpha) * \ln(1-\alpha)}{0.1534}$
	D3 Jander equation for three dimensional diffusion	$\frac{(1-(1-\alpha)^{\frac{1}{3}})^2}{0.04255}$
	D4 Ginstling-Braunshtein equation for three dimensional diffusion	$\frac{1-\frac{2}{3}\alpha-(1-\alpha)^{\frac{2}{3}}}{0.0367}$
Geometrical contraction models	R2 two-dimensional interface controlled	$\frac{1-(1-\alpha)^{\frac{1}{2}}}{0.29289}$
	R3 three-dimensional interface controlled	$\frac{1-(1-\alpha)^{\frac{1}{3}}}{0.20629}$
Nucleation and growth models	F1 JMA- n = 1	$\frac{-\ln(1-\alpha)}{0.6931}$
	F2 JMA- n = 1/2	$\frac{-\ln(1-\alpha)^{\frac{1}{2}}}{0.832}$
	F3 JMA- n = 1/3	$\frac{-\ln(1-\alpha)^{\frac{1}{3}}}{0.8849}$
	F4 JMA- n = 1/4	$\frac{-\ln(1-\alpha)^{\frac{1}{4}}}{0.9124}$
	F5 JMA- n = 2/5	$\frac{-\ln(1-\alpha)^{\frac{2}{5}}}{0.8636}$